Bias effects on the electronic spectrum of a molecular bridge

Heidi Phillips, Alexander Prociuk, and Barry D. Dunietz*

Department of Chemistry, University of Michigan, Ann Arbor, MI 48109

(Dated: June 23, 2010)

Abstract

The effect of bias and geometric symmetry breaking on the electronic spectrum of a model molecular system is studied. Geometric symmetry breaking can either enhance the dissipative effect of the bias, where spectral peaks are disabled, or enable new excitations that are absent under zero bias conditions. The spectral analysis is performed on a simple model system by solving for the electronic response to an instantaneously impulsive perturbation in the dipole approximation. The dynamical response is extracted from the electronic equations of motion as expressed by the Keldysh formalism. This expression provides for the accurate treatment of the electronic structure of a bulk-coupled system at the chosen model Hamiltonian level.

I. INTRODUCTION

Advances in bulk-bridging by nanoscale and molecular scale wire fabrication motivate researchers to explore the function of these systems as electron transporting devices. A wide range of experimental schemes[1–12] are used to fabricate molecular transport junctions, where typically large statistical sampling and elaborate control schemes are required. It therefore remains a challenge to identify a robust, controllable, and reproducible molecular junction fabrication scheme. Computational transport modeling through molecular systems has the potential to address this difficulty and has indeed demonstrated strong conductance dependence on geometric aspects related to the bonding at the interface.[13,14] Proper characterization of bulk-coupled molecular systems is crucial for establishing a meaningful comparison between modeled and measured conductance.

Another promising prospect for enhancing characterization of molecular junctions under bias is offered by combining spectroscopy and current measurements. The charging of a small molecular bridge during the conductance process is coupled with geometric changes of the nuclei. These geometric changes underlie the strong dependence of electron transport (ET) on vibrational degrees of freedom. Experimentally, the vibrational spectra of single molecules are obtained by inelastic electron tunneling spectroscopy (IETS).[15–17] This procedure has been accompanied by substantial progress in modeling phonon-assisted conduction.[18–22] Other experimental developments combine optical spectroscopy with transport studies,[23–27] whereby conductance enhancement in the junction is correlated with changes of the *in situ* measured Raman spectra.

In this study, bias-induced non-equilibrium effects on the electronic spectra of coupled and biased systems are analyzed at the fundamental level. First, we highlight basic bulk-coupling effects on the spectrum of a model molecular system. The electrodes' electronic density of states (DOS) is projected on the junction region, resulting in broadened junction states as illustrated in Figure 1. Secondly, we consider electronic transitions between the electrode-induced energy bands under bias-induced non-equilibrium conditions. The applied bias leads to dynamical flux through the broadened energy levels that disables and enables electronic transitions. Finally, we correlate symmetry breaking modes for the molecular junction and the effect of applied bias on the electronic spectrum.

In the next section we describe our modeling of the spectrum which involves calculating

the junction's electronic density response to an instantaneous impulse in time. The dynamical response is obtained by solving the electronic equations of motion (e.o.m.s) that are expressed using the Keldysh formalism. A time-dependent (TD) first order perturbation theory level (linear response) is used to simplify the expressions. This approach is appropriate to fundamentally treat the electronic response of an electrode-coupled system to TD perturbations. In the following section we describe the method and model used, then we discuss the results and finish with conclusions. Our analysis is performed on a simple model system of a pair of carbon atoms coupled to two gold wires, which allows us to access basic electronic spectral dependence on the applied bias.

II. METHOD

In this section we describe our approach for modeling the electronic spectrum involving electrode-coupled channels under bias conditions. We obtain the electronic spectrum from the dynamic electronic density of a system responding to relevant perturbations. The TD response of the electronic density $\rho(t)$ can be expressed in terms of a TD energy-resolved expression:

$$\rho(t) = \int dE \rho(E,t). \tag{1}$$

The evolving energy-resolved density matrix projected onto the junction is represented by $\rho(E,t)$. *The energy dependence reflects the band structure of the junction coupled with the electrodes. The energy bands have finite widths that support current and, thus, contain scattering states that couple both electrodes.* For example, in this distribution, a DOS peak centered at E' with a ΔE width describes the effectively infinite number of states resulting from the projection. In general, $\rho(E,t)dE$ contributes states to the density matrix ($\rho(t)$) with energies in the range E to $E + dE$.

The time dependent response of this energy density to an instantaneously impulsive pulse in the dipole approximation ($\mathcal{E}_0\delta(t)\hat{D}$, where $\hat{D}$ is the dipole operator) is given by:

$$\langle D(t)\rangle = \int dE \mathrm{Tr}\left[\rho(\mathrm{E,t})\hat{\mathrm{D}}\right]. \tag{2}$$

In this approach, the excitation spectrum of the biased system is contained in the temporal response of the dipole moment ($D(t)$), where peaks in the frequency representation ($\tilde{D}(\Delta\omega) = \int e^{i\Delta\omega t} D(t)dt$) correspond to excitation energies. We now consider, in detail,

the solution to the electronic e.o.m.s as derived using Keldysh formalism. It is, however, important to note the following change in notation: the energy distribution variable, E, is replaced by $\bar{\omega}$, and the time variable, t, by $\bar{t}$, which corresponds to the notation used in an earlier study.[28]

We start from a previously derived representation of the electronic e.o.m., where the electrodes' electronic structure is projected onto the junction region:

$$i\frac{\partial}{\partial \bar{t}}\mathbf{\Delta G}^{<}_{cc}(\bar{t},\bar{\omega}) = [\mathbf{h}_{cc}, \mathbf{\Delta G}^{<}_{cc}(\bar{t},\bar{\omega})] + \int d\omega' [\mathbf{v_{cc}}(\bar{t},\omega')\mathbf{G}^{<}_{cc}(\bar{t},\bar{\omega}-\omega') - \mathbf{G}^{<}_{cc}(\bar{t},\bar{\omega}+\omega')\mathbf{v_{cc}}(\bar{t},\omega')] + \int_{-\infty}^{\infty} dt' [\mathbf{\Sigma^R}(\bar{t}-t')\mathbf{\Delta G_{cc}}^{<}(t',\bar{\omega})e^{-i\mathbf{h_{cc}}(\bar{t}-t')} - e^{i\mathbf{h_{cc}}(\bar{t}-t')}\mathbf{\Delta G_{cc}}(t',\bar{\omega})\mathbf{\Sigma^A}(t'-\bar{t})]. \quad (3)$$

In this equation h_{cc} is the Hamiltonian and $G^<$ is the Green's Function (GF) from which the TD electronic density can be extracted. In the above equation, the subscript cc refers to the central (junction) subspace. Also, this equation and those following are written in atomic units, where $\hbar \equiv 1$. The $G^<$ is separated into time dependent and independent components:

$$G^{<}_{cc}(\bar{t},\bar{\omega}) = G^{0,<}_{cc}(\bar{\omega}) + \Delta G^{<}_{cc}(\bar{t},\bar{\omega}). \quad (4)$$

The bulk projection is based on using the electrode's self-energy expressed by Σ. The full derivation of Eq. (3) is provided in the reference.[28]

Direct propagation of the e.o.m.s is computationally demanding due to the memory effects. Accordingly, we use TD perturbation theory (PT) to solve for the response of the system to the TD perturbation $v(t)$ that is represented by $\Delta G^{<}_{cc}(\bar{t},\bar{\omega})$. As reference for the PT treatment we use the e.o.m. solution under steady biasing conditions ($G^{0,<}_{cc}(\bar{\omega})$). In this approach, the excitation spectrum of the biased system is obtained from the first order electronic response to the instantaneously impulsive perturbing potential (see Eq. 2). The energy distribution, $\mathbf{v_{cc}}(\bar{t},\omega')$, of this TD perturbation acting on the electrode-coupled system, $\mathbf{v}(t)$, is given in terms of the perturbation's Fourier transform, $\tilde{\mathbf{v}}_{\mathbf{cc}}(2\bar{\omega})$:

$$\mathbf{v}_{cc}(\bar{t},\bar{\omega}) = \frac{1}{\pi}e^{-i2\bar{\omega}\bar{t}}\int_{-\infty}^{\infty} dt e^{i(2\bar{\omega})t}\mathbf{v}(t) = \frac{1}{\pi}e^{-i2\bar{\omega}\bar{t}}\tilde{\mathbf{v}}_{\mathbf{cc}}(2\bar{\omega}). \quad (5)$$

We solve the above e.o.m in the full frequency representation, where $\mathrm{G}^{<}(\Delta\omega,\bar{\omega}) \equiv \int_{-\infty}^{\infty} d\bar{t} e^{i\Delta\omega\bar{t}}\mathrm{G}^{<}(\bar{t},\bar{\omega})$. While in the frequency domain-based approach the electrode self-energies can be represented exactly, efficient calculation of the TD PT expansion in the mixed domain-based approach requires a wide band approximation for the electrode self-energies.[28]

The e.o.m. in the full frequency domain takes the following form[29]

$$\sum_{k,l} \boldsymbol{\mathcal{H}}_{ijkl}(\Delta\omega)\boldsymbol{\Delta G}^{<}_{CC,kl}(\Delta\omega,\bar{\omega}) = \left[\mathbf{v}_{CC}(\Delta\omega)\mathbf{G}^{0,<}_{CC}(\bar{\omega}-\Delta\omega/2) - \mathbf{G}^{0,<}_{CC}(\bar{\omega}+\Delta\omega/2)\mathbf{v}_{CC}(\Delta\omega)\right]_{ij}$$
$$+\frac{1}{\pi}\int d\omega' \left[\mathbf{v}_{CC}(2\omega')\boldsymbol{\Delta G}^{<}_{CC}(\Delta\omega-2\omega',\bar{\omega}-\omega') - \boldsymbol{\Delta G}^{<}_{CC}(\Delta\omega-2\omega',\bar{\omega}+\omega')\mathbf{v}_{CC}(2\omega')\right]_{ij}, \tag{6}$$

where

$$\boldsymbol{\mathcal{H}}_{ijkl}(\Delta\omega) \equiv (\Delta\omega + i\eta - \Delta\epsilon_{ij})\delta_{ik}\delta_{jl} - \Gamma_{ijkl}(\Delta\omega). \tag{7}$$

Here, $\Gamma_{ijkl}(\Delta\omega)$ is the broadening function due to coupling to the electrodes, which is generalized to include dynamical effects,

$$\Gamma_{ijkl}(\Delta\omega) \equiv \int dt e^{i\Delta\omega t}\Gamma_{ijkl}(t) = \Sigma^{R}_{ik}(\epsilon_j+\Delta\omega)\delta_{lj} - \Sigma^{A}_{lj}(\epsilon_i-\Delta\omega)\delta_{ik}. \tag{8}$$

In the above equations $\Delta\epsilon_{ij} \equiv \epsilon_i - \epsilon_j$ is the difference between the i-th and j-th eigenvalues (ϵ_i, ϵ_j) of H_{cc}. The implemented formalism includes a broadening factor (η) in defining the tensor $\mathcal{H}$ (see Eq. 7).

In the final expression, which can be expanded to arbitrary order in the perturbation, we express the TD electronic density in terms of the evolving occupations of the projected junction states.[29] The band structure due to the electrode-coupling is included directly in this expansion through the energy distribution variable, $\bar{\omega}$. We note that Eq. (6) involves a tensor of rank four that is contracted with with a matrix (tensor of rank two).

Here, we study the electronic spectrum that can be obtained from the linear response of the electronic density as discussed above. The convolution integral (second term in the RHS of Eq. 6) is dropped in the first order expansion. Using tetradic notation, the tensor $\mathcal{H}_{ijkl}$ of rank four with n dimensionality in each index is re-expressed as a matrix with elements $\mathbf{H}_{ni+j,nk+l}$ and n^2 dimensionality in each index, likewise a matrix becomes a vector. The first order expansion of Eq. (6) then becomes:

$$\mathbf{H}(\Delta\omega)|\boldsymbol{\Delta G}^{<}_{CC}(\Delta\omega,\bar{\omega})\rangle\rangle = |B^{(1)}_{CC}(\Delta\omega,\bar{\omega})\rangle\rangle, \tag{9}$$

where $\mathbf{H}_{ni+j,nk+l}(\Delta\omega) \equiv \boldsymbol{\mathcal{H}}_{ijkl}(\Delta\omega)$, and $|\boldsymbol{\Delta G}^{<}_{CC}(\Delta\omega,\bar{\omega})\rangle\rangle_{ni+j} \equiv \boldsymbol{\Delta G}^{<}_{CC,ij}(\Delta\omega,\bar{\omega})$. The first order response matrix is given by:

$$|B^{(1)}_{CC}(\Delta\omega,\bar{\omega})\rangle\rangle_{ni+j} \equiv \left[\tilde{\mathbf{v}}_{CC}(\Delta\omega)\mathbf{G}^{0,<}_{CC}(\bar{\omega}-\Delta\omega/2) - \mathbf{G}^{0,<}_{CC}(\bar{\omega}+\Delta\omega/2)\tilde{\mathbf{v}}_{CC}(\Delta\omega)\right]_{ij}. \tag{10}$$

At the steady state, any transient or TD aspects due to applied bias are completely dissipated. The steady state description, which is used as the reference for the perturbation treatment, is achieved by a proper time independent limit of the above treatment, where the corresponding time independent perturbation $\mathbf{v}(t) \equiv \mathbf{v}_\circ$ is Fourier transformed as in Eq. (6) to the frequency domain:

$$\mathbf{v}(\Delta\omega) = 2\pi\delta(\Delta\omega)\mathbf{v}_\circ\,. \tag{11}$$

For the steady state, the two-frequency based representation of the e.o.ms is collapsed to a single variable expansion. The resulting expression describes a time independent correction to the unbiased system represented by $G^{0,<}$:

$$|\mathbf{G}^{0,<}_{CC}(\bar{\omega})\rangle\rangle \rightarrow |\mathbf{G}^{0,<}_{CC}(\bar{\omega})\rangle\rangle + \mathbf{G}(0)|B^{(1)}_{CC}(\bar{\omega})\rangle\rangle, \tag{12}$$

where $B^{(1)}_{CC}$ is contracted with $\mathbf{G}(0)$, and in the steady state limit is given by

$$|B^{(1)}_{CC}(\bar{\omega})\rangle\rangle_{ni+j} \equiv \left[\mathbf{v}_\circ\mathbf{G}^{0,<}_{CC}(\bar{\omega}) - \mathbf{G}^{0,<}_{CC}(\bar{\omega})\mathbf{v}_\circ\right]_{ij}\,. \tag{13}$$

In calculating $\mathbf{G}^{0,<}_{CC}(\bar{\omega})$, we use the relationship between $\mathbf{G}^{<}(\bar{\omega})$ and the retarded GF, $\mathbf{G}^{R}(\bar{\omega})$, which entails calculating the Fermi-matrix.[28]

III. MODELS

The electronic spectra of biased molecular junctions are studied using the model system illustrated in Figure 2. The simple model consists of a one-dimensional wire as the electrode and two sites oriented perpendicularly to the wires as the junction. Each site is described using a single s-type basis function, which is expressed in spherical coordinates relative to the center of each atom. The spherical function size is set to the electronic radius of a gold atom (for wire sites) or carbon atom (for the junction sites).

The Hamiltonian of the system is divided as usual into three parts: the left and right electrodes and the junction region. The junction region, shown in Fig. 2, consists of the two carbon atoms and three gold atoms from each electrode. Within this region we identify a "core" region consisting of the two carbon atoms and the two center gold atoms between which the carbons are situated. The gold atoms within the wire are spaced 2.88 Angstroms apart and the two core gold atoms are spaced 1.90 Å apart. The carbon bond length is set to 3.29 Å. In a previous study we found that this "diamond" like structure at the simple

model Hamiltonian level provides an opportunity to probe the electronic spectrum of an electrode-coupled system affected by an applied bias.

The atomic orbital Hamiltonian matrix is parametrized based on the ionization potential and evaluated using the following Huckel-type expressions:

$$H_{A,A} = -I_A, \tag{14}$$

$$H_{A,B} = -\frac{1}{2}K(I_A + I_B)S_{A,B}, \tag{15}$$

where $S_{A,B}$ is the atomic orbital overlap between the s-electron basis functions centered on atoms A and B, I_A is the ionization potential for atom A, and K is a constant set to 1.75. The numerical values for these parameters are provided in Table I. The Hamiltonian is then orthogonalized ($\mathbf{H} \rightarrow \mathbf{S}^{-1/2}\mathbf{H}\mathbf{S}^{-1/2}$) followed by the imposition of a tight-binding condition within the electrode regions, where only on-site and nearest-neighbor hopping elements are non-zero. All site and hopping elements are kept in the four-site region of the orthogonalized Hamiltonian that corresponds to the Au-C_2-Au region of the pre-orthogonalized Hamiltonian. This Hamiltonian is padded with electrode wires of nine gold atoms on each side of the perpendicular C_2 system to ensure that edge effects are minimized in the orthogonalization procedure.

A steady potential bias is applied by chemical potential shifts from the Fermi energy with an opposite sign on each of the electrodes as shown in Fig. 2. In this study, the electronic spectrum is calculated for the dipole moment oriented along the C-C bond (y-axis). The electronic DOS of the device region at equilibrium (zero applied-bias) are shown in Figures 3 and 4 (left). As discussed below, in the first figure we consider the electronic spectrum affected by electrode-induced electronic DOS broadening, and in the second figure we consider geometrically-induced symmetry breaking effects. In all calculations, the energy scale is shifted to set the Fermi energy to zero for convenience.

IV. RESULTS

We first study the electrode-coupling effect (broadening of energy states) on the electronic spectrum. The electronic spectrum of the coupled system is provided in Figure 3 (right). We focus on the broadening effect, which can be tuned by the fundamental broadening factor in calculating the retarded GF, $\mathbf{G}^R(\bar{\omega})$, of the electrode-coupled system. The broadening of

the electronic DOS leads to broadening of the main spectral peak related to the transition between the highest occupied molecular orbital (HOMO) and lowest unoccupied molecular orbital (LUMO) orbitals. An additional widely broadened peak is observed at lower spectral frequencies and is associated with the band of states in the DOS located energetically between the HOMO and LUMO peaks.

We also study the combined effect of bias and molecular scale motion on the spectrum. The carbon atoms are shifted by increments of 0.19 Å toward either electrode, where the resulting molecular electronic DOS is provided in Figure 4. The two occupied states respond only slightly to the carbon shift. More substantial changes are observed for the virtual state energies, where a larger, positive shift of the higher virtual state is noted. The corresponding spectra are provided in Fig. 4 (right). Upon the symmetry breaking shift, the symmetry forbidden HOMO-Virt2 transition becomes allowed (Virt2 denotes the higher unoccupied state, which is the LUMO+1). The two spectral peaks are shifted to higher and lower values in energy, corresponding to the changes in the virtual state energy.

It is important to comment on the HOMO-LUMO transition, where symmetry-induced disabling effects are noted. The molecular orbital picture for the core region at equilibrium (no bias applied) is provided in Figure 5. The orbital energies, corresponding to Fermi energy of -8.067 eV, are provided along with the orbital assignment. The even/odd symmetry of the original orbitals is broken when the carbons are shifted toward the electrode. Clearly, at equilibrium, shifting the carbon atoms toward either electrode has the same effect on the electronic DOS and therefore on the spectrum. Next we consider the electronic spectrum under applied bias.

Potential bias is applied to the geometrically symmetric system in increments of 2V. The resulting flux populates and depopulates the virtual and occupied orbitals respectively. Specifically, the electron flux partially occupies the LUMO and partially depletes the HOMO, affecting the spectrum fundamentally. First, the spectral cross section of the corresponding allowed excitation in the unbiased system is reduced. As the bias is increased, the HOMO-LUMO transition is disabled as illustrated in Figure 6. The dynamical occupation of the orbitals also affects the spectrum by enabling new transitions that are otherwise absent for the unbiased system. Upon bias induced flux, the Occ1-HOMO transition becomes enabled and increases with increasing applied bias (Occ1 denotes the lower occupied, or HOMO-1 state).

On a side note, we confirm the assignment of the bias-enabled peak to the Occ1-HOMO excitations. The same peak appears in the spectrum of a model device that includes only one gold atom on each side, as shown under biases ranging from 0 to 6V (insert to Fig. 6). This model, while insufficient for converging the representation of electrode-coupling, confirms that the additional peaks in the low energy regime are assigned only to intra-gold wire transitions (Fig.6).

We now consider the application of bias potential to the shifted (symmetry broken) carbon systems. Figures 7(a) and (b) show the spectra when the carbons are shifted toward the source and drain electrode, respectively. We focus on the effect of potential bias on the HOMO-LUMO transition for different geometric shifts. The bias-disabling of this transition is enhanced when the carbons are shifted toward the source. The opposite effect occurs when the symmetry breaking involves a shift toward the drain. In this case, the bias-disabling is diminished and the spectrum features a small increase of the bias-induced peak as well as a shift to higher excitation energies.

To understand the reason for this difference, we reconsider the electronic orbitals illustrated in Fig. 5 in relation to applied bias. For example, we focus on the LUMO where the symmetry breaking results in a shift of the projected density to the more *distant* gold atom. The symmetry breaking-induced polarization is enhanced, therefore, by flux-induced polarization when the molecule is shifted toward the source. On the other hand, the flux negates the symmetry breaking-induced polarization of the LUMO when the carbons are shifted toward the drain. Therefore, the bias-disabling effect on the HOMO-LUMO spectral peak is enhanced when the geometric shift is oriented toward the source and is decreased when the shift is oriented toward the drain.

The symmetry breaking is more subtle in the case of the occupied orbital transitions. Unlike the LUMO, the symmetry breaking shifts the projected density toward the *closer* gold atom. This slight symmetry breaking of the occupied orbitals is reversed by bias-induced flux upon shifting the carbons toward the source and is enhanced when the carbons are shifted toward the drain. Enabling of the Occ1-HOMO transition requires that the HOMO level becomes (at least partially) unoccupied. We find that increasing bias enhances the bias-enabled Occ1-HOMO peak for the geometric shift toward the drain. This peak appears and then is reduced with further increase in bias for the shift toward the source.

V. CONCLUSIONS

The effects of electrode-coupling and bias on the electronic spectrum of a simple molecular model system are analyzed. Fundamentally, electrode-coupling leads to broadened electronic spectral peaks. Furthermore, biasing conditions can lead to substantial changes in the electronic spectrum. Under bias, spectral peaks can be enabled by the dynamical occupation and depletion of levels due to the electron flux. The dynamical occupation will therefore reduce spectral peaks that are present at equilibrium conditions but can also enable additional transitions, for example, those between equilibrium occupied levels. Symmetry breaking molecular motion fundamentally affects the spectrum by enabling symmetry forbidden transitions. The bias effect on the spectrum can be negated or enhanced by this symmetry breaking of molecular orbitals.

VI. ACKNOWLEDGMENTS

BDD work was supported as part of the Center for Solar and Thermal Energy Conversion, an Energy Frontier Research Center funded by the U.S. Department of Energy, Office of Science, Office of Basic Energy Sciences under Award Number DE-SC0000957. HP is thankful for support from the University of Michigan Rackham Graduate School Summer Institute and the University of Michigan Rackham Merit Fellowship.

* Electronic address: bdunietz@umich.edu

[1] L. A. Bumm, J. J. Arnold, M. T. Cygan, T. D. Dunbar, T. P. Burgin, L. I. Jones, D. L. Allara, J. M. Tour, and P. S. Weiss, *Science* **271**, 1705 (1996).

[2] M. A. Reed, C. Zhou, C. J. Muller, T. P. Burgin, and J. M. Tour, *Science* **278**, 252 (1997).

[3] R. E. Holmlin, R. Haag, M. L. Chabinyc, R. F. Ismagilov, A. E. Cohen, A. Terfort, M. A. Rampi, and G. M. Whitesides, *J. Am. Chem. Soc.* , 5075 (2001).

[4] X. D. Cui, A. Primak, X. Zarate, J. Tomfohr, O. F. Sankey, A. L. Moore, T. A. Moore, D. Gust, G. Harris, and S. M. Lindsay, *Science* **294**, 571 (2001).

[5] J. Reichert, R. Ochs, D. Beckmann, H. B. Weber, M. Mayor, and H. v. Löhneysen, *Phys. Rev. Lett.* **88**, 176804 (2002).

[6] J. G. Kushmerick, D. B. Holt, S. K. Pollack, M. A. Ratner, J. C. Yang, T. L. Schull, J. Naciri, M. H. Moore, and R. Shashidhar, *J. Am. Chem. Soc.* **124**, 10654 (2002).

[7] J. K. N. Mbindyo, T. E. Mallouk, J. B. Mattzela, I. Kratochvilova, B. Razavi, T. N. Jackson, and T. S. Mayer, *jacs* (2002).

[8] B. Q. Xu and N. Tao, *Science* **301**, 1221 (2003).

[9] B. Q. Xu, X. Y. Xiao, X. Yang, L. Zang, and N. J. Tao, *J. Am. Chem. Soc.* **127**, 2386 (2005).

[10] X. Guo, J. P. Small, J. E. Klare, Y. Wang, M. S. Purewal, I. W. Tam, B. H. Hong, R. Caldwell, L. Huang, S. O'Brien, J. Yan, R. Breslow, S. J. Wind, J. Hone, P. Kim, and C. Nuckolls, *Science* **311**, 356 (2006).

[11] J. Y. Tang, Y. L. Wang, J. E. Klare, G. S. Tulevski, S. J. Wind, and C. Nuckolls, *Angew. Chem. Int. Ed.* **46**, 3892 (2007).

[12] X. Chen, Y.-M. Jeon, J.-W. Jang, L. Qin, F. Huo, W. Wei, and C. A. Mirkin, *J. Am. Chem. Soc.* , 8166 (2008).

[13] H. Basch, R. Cohen, and M. A. Ratner, *Nano. Lett.* **5**, 1668 (2005).

[14] T. Perrine and B. D. Dunietz, *Phys. Rev. B* **75**, 195319 (2007).

[15] W. Ho, *The Journal of Chemical Physics* **117**, 11033 (2002).

[16] W. Wang, T. Lee, I. Kretzschmar, and M. A. Reed, *Nano. Lett.* **4**, 643 (2004).

[17] Y. Selzer, L. Cai, M. A. Cabassi, Y. Yao, J. M. Tour, T. S. Mayer, and D. L. Allara, *Nano. Lett.* **5**, 61 (2005).

[18] M. Galperin, M. Ratner, and A. Nitzan, *J. Chem. Phys.* **121**, 11965 (2004).

[19] N. Sergueev, D. Roubtsov, and H. Guo, *Phys. Rev. Lett.* **95**, 146803 (2005).

[20] C. H artle, R. abd Benesch and M. Thoss, *Phys. Rev. Lett.* **102**, 146801 (2009).

[21] D. A. Ryndyk, M. Hartung, and G. Cuniberti, *Phys. Rev. B* **73**, 045420 (2006).

[22] M. Galperin, M. A. Ratner, and A. Nitzan, *Journal of Physics: Condensed Matter* **19**, 103201 (81pp) (2007).

[23] A. M. Nowak and R. L. McCreery, *J. Am. Chem. Soc.* **126**, 16621 (2004).

[24] A. M. Nowak and R. L. McCreery, *Analytical Chemistry* **76**, 1089 (2004).

[25] A. P. Bonifas and R. L. McCreery, *Chemistry of Materials* **20**, 3849 (2008).

[26] D. R. Ward, N. J. Halas, J. W. Ciszek, J. M. Tour, Y. Wu, P. Nordlander, and D. Natelson, *Nano. Lett.* **8**, 919 (2008).

[27] D. R. Ward, G. D. Scott, Z. K. Keane, N. J. Halas, and D. Natelson, *J. Phys.: Condens. Matter* **20**, 374118 (2008).

[28] A. Prociuk and B. D. Dunietz, *Phys. Rev. B* **78**, 165112 (2008).

[29] A. Prociuk, H. Phillips, and B. D. Dunietz, *J. Phys.: Conf. Ser.* **220**, 012008 (2010).

Atom	*radius Å*	I_A *(eV)*	α *(Å^{-2})*
C	0.77	11.26	1.074
Au	1.44	9.22	0.307

TABLE I: Radii, ionization potentials, I_A, and Gaussian basis set coefficients, α, for C and Au

FIG. 1: Effect of coupling discrete molecular states to band structured bulk material

FIG. 2: Schematic diagram representing junction region. Effect of potential bias is implied as well as the shift of carbons toward source or drain electrode

FIG. 3: (a) The electronic DOS under increasing broadening factor. (b) The electronic spectra corresponding to increasing broadening factor.

FIG. 4: (a) The electronic DOS under carbon shifting toward an electrode at equilibrium. (b) The electronic spectra under the carbon shifting. The Homo-Virt2 transition is enabled by the symmetry breaking.

FIG. 5: Molecular orbital diagrams for: (a) non-shifted case and shift of 0.38 Å (b) toward source electrode, (c) toward drain electrode. Relevant bond lengths and energies are included.

FIG. 6: Spectral dependence on increasing potential bias for geometrically symmetric junction. (Inset) Bias dependence for small device region, indicates cause of Au-Au interaction.

FIG. 7: The spectral dependence on increasing bias under carbon shift toward (a) source electrode, (b) drain electrode.

FIG. 1:

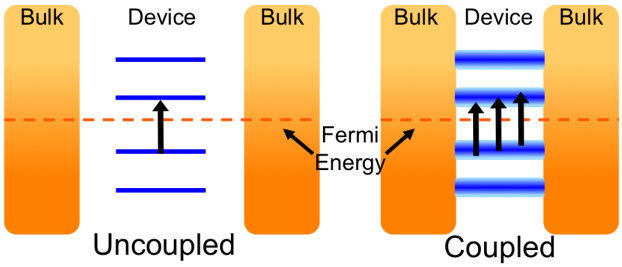
Bulk
Device
Bulk
Fermi
Energy
Uncoupled
Bulk
Device
Bulk
Coupled

FIG. 2:

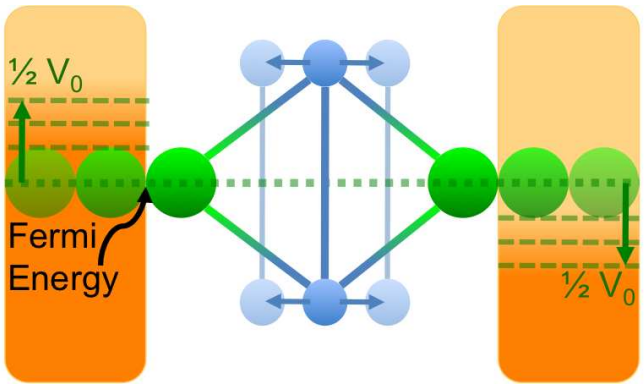

FIG. 3:

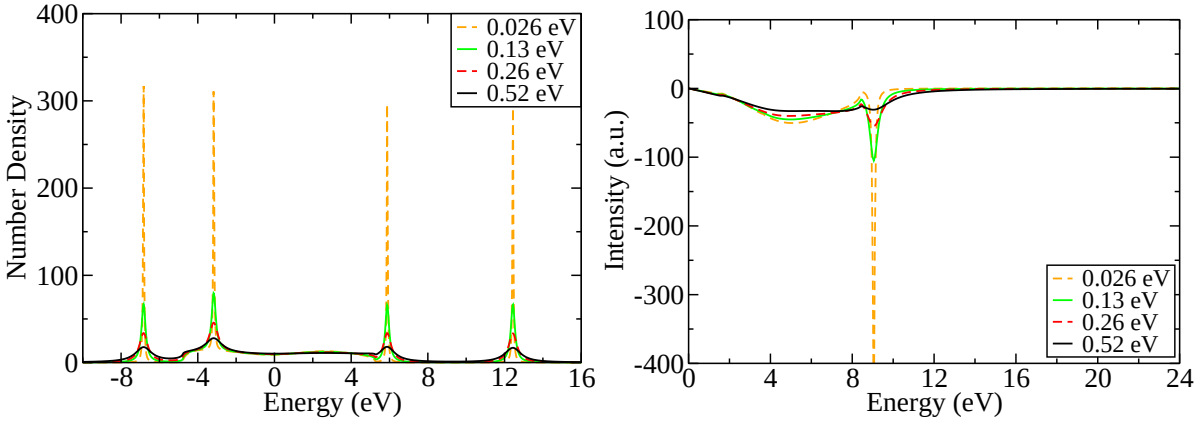
Number Density
Energy (eV)
0.026 eV
0.13 eV
0.26 eV
0.52 eV
Intensity (a.u.)
Energy (eV)
0.026 eV
0.13 eV
0.26 eV
0.52 eV

FIG. 4:

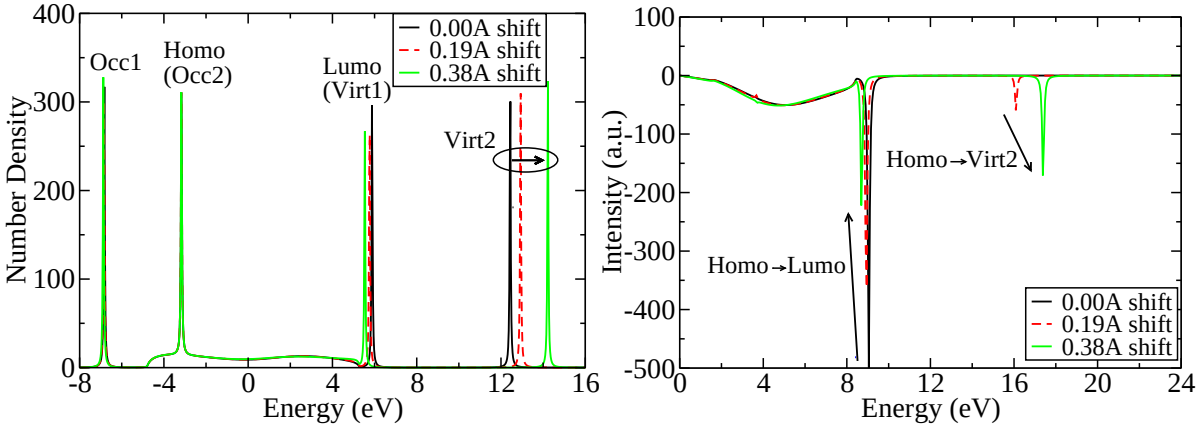
Number Density
Energy (eV)
Occ1
Homo
(Occ2)
Lumo
(Virt1)
Virt2
0.00A shift
0.19A shift
0.38A shift
Intensity (a.u.)
Homo→Virt2
Homo→Lumo

FIG. 5:

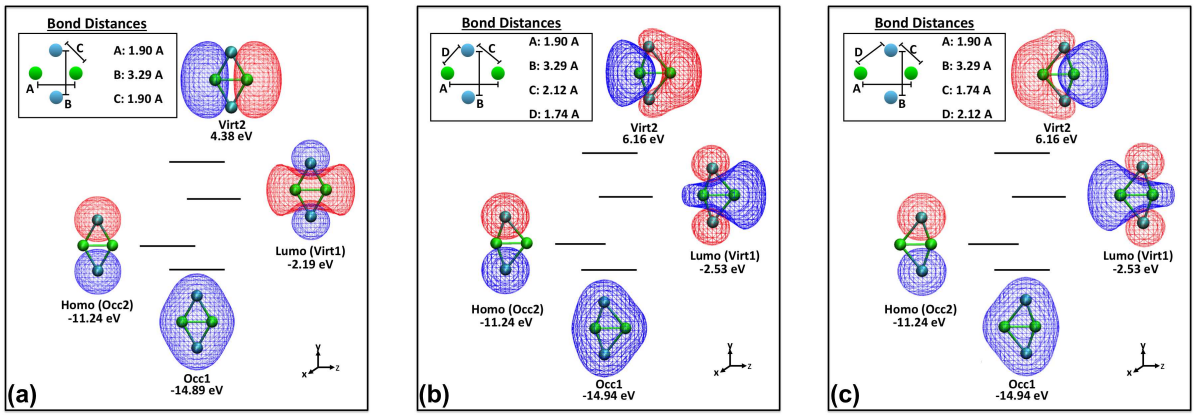
Bond Distances
A: 1.90 A
B: 3.29 A
C: 1.90 A
Virt2
4.38 eV
Lumo (Virt1)
-2.19 eV
Homo (Occ2)
-11.24 eV
Occ1
-14.89 eV
(a)
Bond Distances
A: 1.90 A
B: 3.29 A
C: 2.12 A
D: 1.74 A
Virt2
6.16 eV
Lumo (Virt1)
-2.53 eV
Homo (Occ2)
-11.24 eV
Occ1
-14.94 eV
(b)
Bond Distances
A: 1.90 A
B: 3.29 A
C: 1.74 A
D: 2.12 A
Virt2
6.16 eV
Lumo (Virt1)
-2.53 eV
Homo (Occ2)
-11.24 eV
Occ1
-14.94 eV
(c)

FIG. 6:

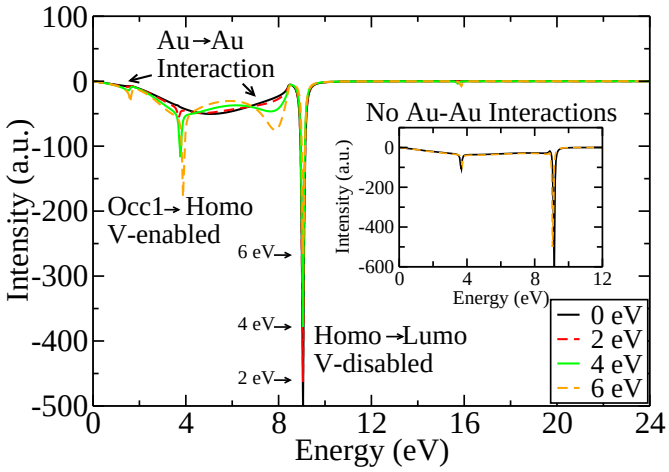
Au→Au
Interaction
Occ1→ Homo
V-enabled
6 eV→
4 eV→
2 eV→
Homo →Lumo
V-disabled
No Au-Au Interactions
Intensity (a.u.)
Energy (eV)
0 eV
2 eV
4 eV
6 eV
Intensity (a.u.)
Energy (eV)

FIG. 7:

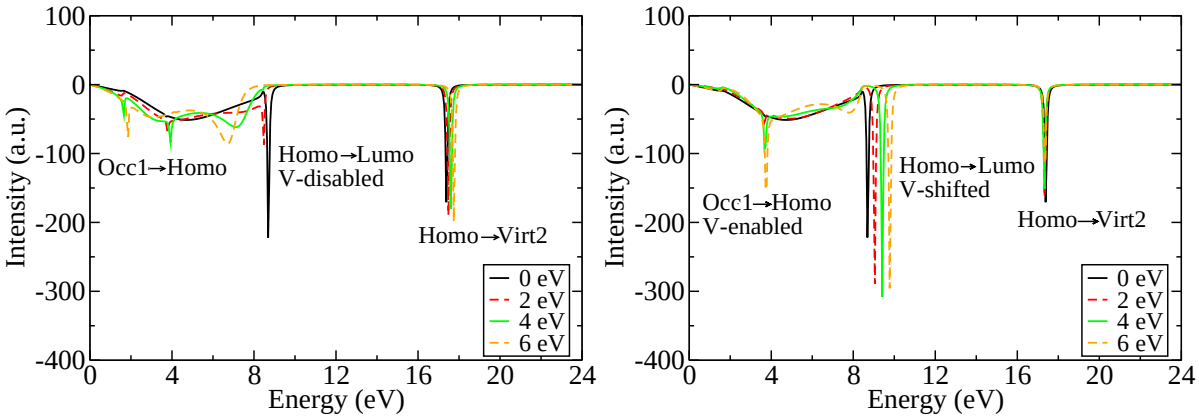
Intensity (a.u.)
Energy (eV)
Occ1→Homo
Homo→Lumo
V-disabled
Homo→Virt2
0 eV
2 eV
4 eV
6 eV
Occ1→Homo
V-enabled
Homo→Lumo
V-shifted
Homo→Virt2